Int J Adv Manuf Technol (2017) 89:2355–2362
DOI 10.1007/s00170-016-9280-2

ORIGINAL ARTICLE

Study on surface appearance, geometry size, and delta-ferrite content of ZrO_2-aided TIG welding of AISI 316LN stainless steel

Kuang-Hung Tseng[1]

Received: 3 May 2016 / Accepted: 1 August 2016 / Published online: 11 August 2016

Abstract This study investigated the influence of oxide with a more negative Gibbs free energy (ΔG) on the surface appearance, geometry size, and delta-ferrite (δ-Fe) content of AISI 316LN stainless steel subjected to flux-aided tungsten inert gas (TIG) welding. Powdered ZrO_2 of various particle sizes mixed with 80 % water/20 % acetone solution was used as flux. The potential advantages of ZrO_2-aided TIG welding were also demonstrated. The results show that nanoscale ZrO_2 flux produces a TIG weld with a slag-free surface, but it did not significantly increase the depth-to-width ratio of the weld. The present work also found that ZrO_2 flux slag influences the δ-Fe content of AISI 316LN stainless steel weld. ZrO_2-aided TIG welding has low tendency to form undercut ting and allows high-speed welding. The potential advantages of the ceramic slag created by the ZrO_2 flux are a small temperature difference between the center and edges of welding pool surface, a low solidified rate of liquid metal at the rear of the welding pool, as well as alleviation of the arc pressure at the front of the welding pool.

Keywords Undercutting · Flux slag · Powdered ZrO_2 · Stainless steel · High-speed welding

1 Introduction

The penetration depth is an important quality characteristic of metals that are to be welded in a single-pass operation [1], as it determines the welding productivity. TIG welding is one of the popular arc welding technologies. However, this technology operates in melt-in (conduction limited) mode; thus, the conduction of heat energy from an electric arc through the metal strongly affects the shape and size of the resultant weld. As a result, the penetration depth of TIG weld is limited. The penetration depth achievable in a single-pass, autogenous operation of TIG welding of stainless steel with no edge preparation is less than 3 mm [2, 3]; thus, the use of TIG welding to join thick-section metals is not cost-efficient. The solution to this issue is often increasing the welding current. Unfortunately, the resultant weld becomes excessively wide and slightly gains depth when the welding current increases [4]. Coarse grains also form in the heat-affected zone. These problems have therefore attracted considerable research into and much industrial interest in the flux-aided TIG welding since the late 1980s. In the flux-aided TIG welding technique, a thin layer of flux is coated on the surface of metal plates or tubes to be welded, and a single-pass welding with no filler metal is subsequently performed to achieve a high-penetration capability. The use of flux in TIG welding represents a substantial technique upgrade that saves time and reduces cost.

The ingredient of the flux plays a key role in improving the penetration depth of TIG weld. It is selected according to the metal to be welded [5]. For instance, a flux consisting of 6 % Fe_2O_3, 60 % Cr_2O_3, 22 % TiO_2, and 12 % TiO has been reported for plain carbon steel [6]; a flux consisting of 30–50 % TiO_2, 25–40 % SiO_2, 10–20 % Cr_2O_3, 5–15 % NiO, and 5–15 % CuO has been reported for austenitic stainless steel [7]; a flux ingredient consisting of 40–80 % B_2O_3, 5–20 % SiO_2, 5–20 % Cr_2O_3, 1–15 % TiO_2, 1–15 % KCl, and 1–5 % Al_2O_3 has been reported for ferritic stainless steel [8]. When fluxes were used in TIG welding of steels, oxides with less negative ΔG, except Al_2O_3, were observed to result in a significant increase in penetration depth of the welds [9].

✉ Kuang-Hung Tseng
tkh@mail.npust.edu.tw

[1] Institute of Materials Engineering, National Pingtung University of Science and Technology, No. 1, Hseuhfu Rd., Neipu Pingtung 91201, Taiwan

Empirical data on the influence of oxides with more negative ΔG, in particular ZrO_2, on the shape and size of TIG welds are limited. Therefore, much research is required to understand fully the characteristics of ZrO_2 flux that are used in TIG welding of steels.

The productivity of conventional TIG welding can be improved by increasing the travel speed [10]. However, this approach is limited by undercutting formation. Undercutting is the most common shape imperfection in welding fabrication; it creates a groove that melts into the base metal adjacent to the weld toe and remains unfilled by the liquid metal [11]. Undercutting thus causes a notch at the toe of the weld, which significantly reduces the fatigue strength of the weldment by increasing stress concentration at the tip of the notch. The undercutting defect generated by high-speed fusion welding ultimately compromises the weld soundness, thus imposing an upper limit to the travel speed that can be used for fusion welding [12]. An in-depth understanding of undercutting formation is therefore needed to develop process modifications that decrease the tendency for imperfect shape and to attain higher welding productivity and quality levels.

The present study investigated the effect of ZrO_2 flux of various particle sizes on the surface appearance, geometry size, and δ-Fe content of TIG welds, and the results were compared. This investigation also examined the influence of welding current and travel speed on the undercutting generated by conventional TIG welding. The main purpose here is to reveal that the undercutting defect can be effectively eliminated by using ZrO_2-aided TIG welding technique. Ultimately, this knowledge in practice will contribute to the development of a multicomponent ZrO_2-based flux that is suitable for high-speed TIG welding of steels, resulting in a higher penetration depth of the weld with no undercutting.

2 Experimental details

AISI 316LN stainless steel was used as the base metal. It is a nitrogen-alloyed ultralow-carbon austenitic stainless steel that is a common material for main pipelines in nuclear power plants. Larger specimen sizes generally result in high cooling rates in the resultant weldment; size thus highlights the effect of the flux on the shape and size of the resultant weld. In the present work, the rectangular specimens (160-mm length, 150-mm width) were cut from stainless steel plates with 6-mm thickness. Prior to welding, all specimens were lightly ground with 320-grit sandpaper.

Average particle sizes of powdered ZrO_2 were differentiated into three discrete grades: 45 μm (microscale grade), 0.3 μm (submicroscale grade), and 25 nm (nanoscale grade). Figure 1 shows the preparation process for obtaining flux coating. A constant weight of ZrO_2 powder was mixed with a constant weight of 80 % water/20 % acetone solution in a beaker, and then, the mixture was stirred with a spoon to form a paint-like flux. The flux was then coated onto the surface of the specimen by using a paintbrush. The solution immediately volatilized, leaving a coating of ZrO_2 flux on the surface of AISI 316LN stainless steel plate.

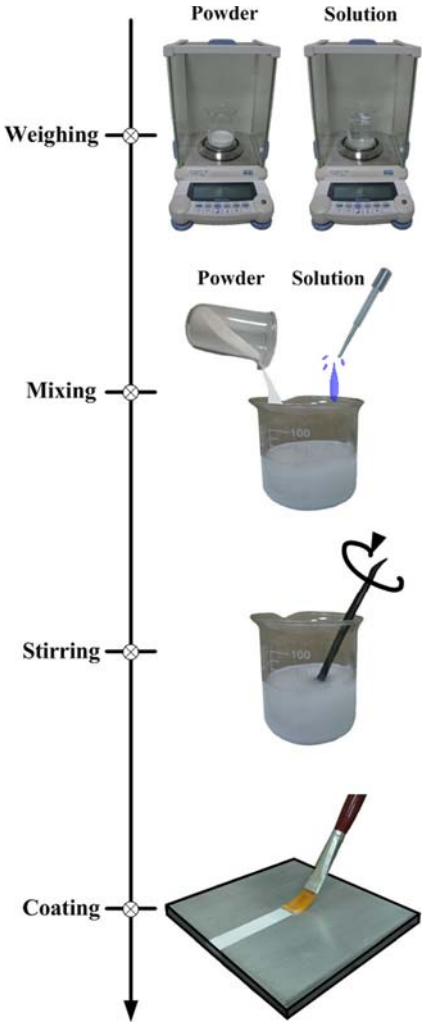

Fig. 1 Preparation process for obtaining flux coating

A single-pass, autogenous TIG welding using semi-automatic equipment was carried out. A direct current welding machine with a constant current mode of power supply was used to produce a bead-on-plate weld. A water-cooled welding torch was carried on a linear guideway and was moved perpendicularly along the centerline of the specimen. A 1.5 % lanthanated tungsten electrode (AWS classification EWLa-1.5) having a rod diameter of 3.2 mm and an included grind angle of 60° was used to create an electric arc. The distance between the electrode tip and the specimen surface was kept at 2 mm. Commercial grade argon gas was used to create a protective inert atmosphere during welding.

The Fischer feritscope was used to measure the δ-Fe content in the weld. This device detects phases such as ferrite according to the magnetic susceptibility, which differs from

that of paramagnetic austenite [2]. To minimize measurement errors resulting from inhomogeneity in the weld, the average value of seven measurements taken from various locations along the welded surface was calculated. The Olympus stereo microscope was used to photograph the surface appearance of the weld. The weldment was cut at a section perpendicular to the welding direction and then mounted. The mounted samples were ground with SiC abrasives, polished with Al_2O_3 suspensions, and then subjected to electrolytic etching. The Mitutoyo toolmaker's microscope was used to measure penetration depth and bead width of the weld. The Leco elemental analyzer was used to measure oxygen concentration in the weld. In the present work, each datum represents the average of two samples for a given weldment or three positions for a given weld.

3 Results and discussion

3.1 Surface appearance of TIG welds produced with different ZrO_2 particle sizes

Figure 2 shows the surface appearance of AISI 316LN stainless steel TIG welds produced with and without ZrO_2 flux at a welding current of 200 A and at a travel speed of 150 mm/min. No undercutting formed at the toe of the weld. Figure 2a shows the results of TIG welding without ZrO_2 flux, which created a metallic surface of AISI 316LN stainless steel weld. A large amount of slag was produced with the use of microscale ZrO_2 flux (Fig. 2b). In contrast, a small amount of slag was produced with the use of submicroscale ZrO_2 flux (Fig. 2c). ZrO_2 flux eventually reacted with impurities, forming molten slag with density lower than that of molten iron. The flux slag covered the welded surface after cooling. Figure 2d shows the results of TIG welding with nanoscale ZrO_2 flux, which produced a slag-free welded surface. Pawlow [13] reported that the melting temperature of the particle decreases with its size because of the high surface-area-to-volume ratio of small particles and the low coordination number of atoms at the particle surface. This attribute indicates that the melting temperature of nanoscale particles is lower than that of microscale or submicroscale particles. Consequently, the arc heat of TIG welding is sufficient to fully melt the flux coating of nanoscale ZrO_2, resulting in a satisfactory appearance of AISI 316LN stainless steel TIG welded surface. Figure 3 shows a scanning electron microscope (SEM) micrograph of incompletely melted flux located at the sides of the welded surface. The image suggests that incompletely melted ZrO_2 flux with some particles accumulates on both sides of the TIG welded surface. This pattern of accumulation is due to the temperature of the outer regions of the TIG welding arc, which is far lower than the melting temperature of the powdered ZrO_2 and thus results in a large amount of incompletely melted ZrO_2 particles.

3.2 Geometry size of TIG welds produced with different ZrO_2 particle sizes

Figure 4 shows the geometry size of AISI 316LN stainless steel TIG welds produced with and without ZrO_2 flux at a

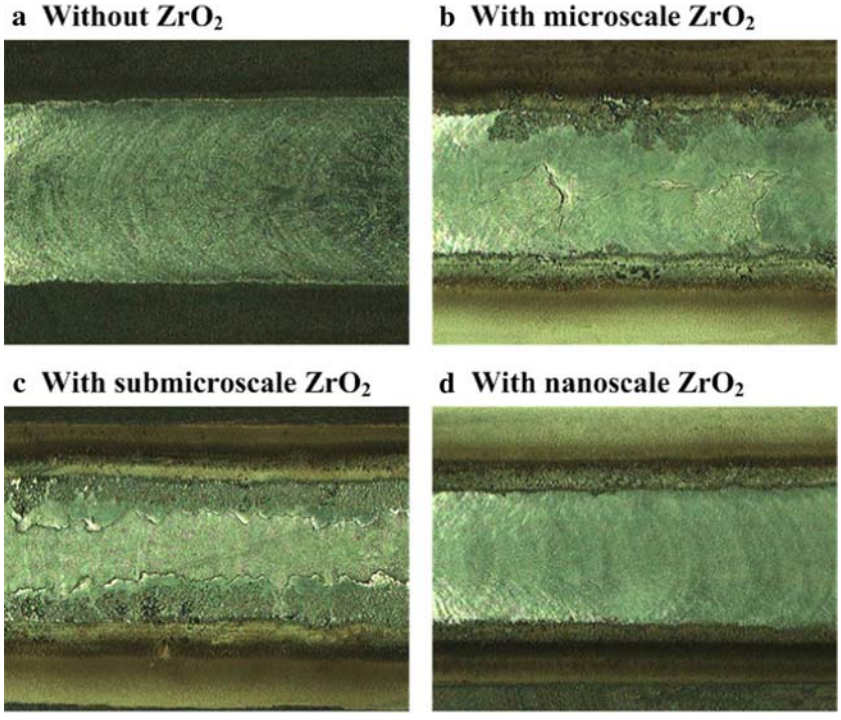

Fig. 2 Surface appearance of TIG welds produced with and without ZrO_2 at a welding current of 200 A and a travel speed of 150 mm/min

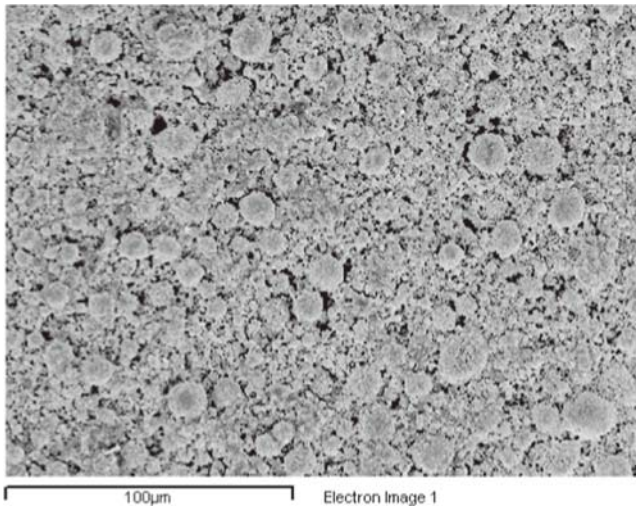

Fig. 3 SEM micrograph of incomplete melted flux located at sides of welded surface

welding current of 200 A and a travel speed of 150 mm/min. In the TIG weld produced without ZrO_2 flux, the penetration depth and bead width were 1.26 and 9.51 mm, respectively. Compared with the TIG weld produced without ZrO_2 flux, TIG welds produced with microscale and submicroscale ZrO_2 fluxes exhibited a shallower depth and wider width. TIG weld produced with nanoscale ZrO_2 flux exhibited a greater depth and narrower width. These results thus imply that nanoscale ZrO_2 flux does not contribute to an increase in the depth-to-width ratio of AISI 316LN stainless steel TIG weld. The flow of liquid metal in the welding pool, in particular, thermocapillary force (F_{tc}) and electromagnetic force (F_{em}), affects the shape and size of the weld. Tseng and Chen [14] reported that F_{tc} dominates the inward or outward liquid metal convection along the welding pool surface, whereas F_{em} dominates the downward liquid metal convection in the welding pool.

There were substantial temperature differences across the free surface of the welding pool. The variation of the surface tension gradient caused liquid metal to flow along the welding pool surface from the low-tension region to the high-tension region. In the absence of oxygen in the welding pool of the iron-based alloys, the tension in the welding pool surface decreased with increasing temperature. In this case, the surface tension was highest at the edges of the welding pool surface and lowest at the center of the welding pool surface, resulting in a radially outward F_{tc}. At low concentrations of oxygen in the welding pool of the iron-based alloys, the tension in the welding pool surface increased with increasing temperature. In this case, the surface tension was highest at the center of the welding pool surface and lowest at the edges of the welding pool surface, resulting in a radially inward F_{tc}. Lu et al. [15] reported that when the effective oxygen concentration in austenitic stainless steel TIG weld is within 70–300 ppm, the surface tension of liquid iron increases with increasing temperature; otherwise, the surface tension of liquid iron decreases with increasing temperature. Figure 5 shows the average oxygen concentration in AISI 316LN stainless steel TIG welds produced with and without ZrO_2 flux. The results show that average oxygen concentration in the weld produced without ZrO_2 flux was 44 ppm. The average oxygen concentration did not substantially increase in AISI 316LN stainless steel TIG welds produced with different ZrO_2 particle sizes; thus, the direction of F_{tc} in the welding pool was still radially outward. These results clearly suggest that ZrO_2 flux has very weak activating potency.

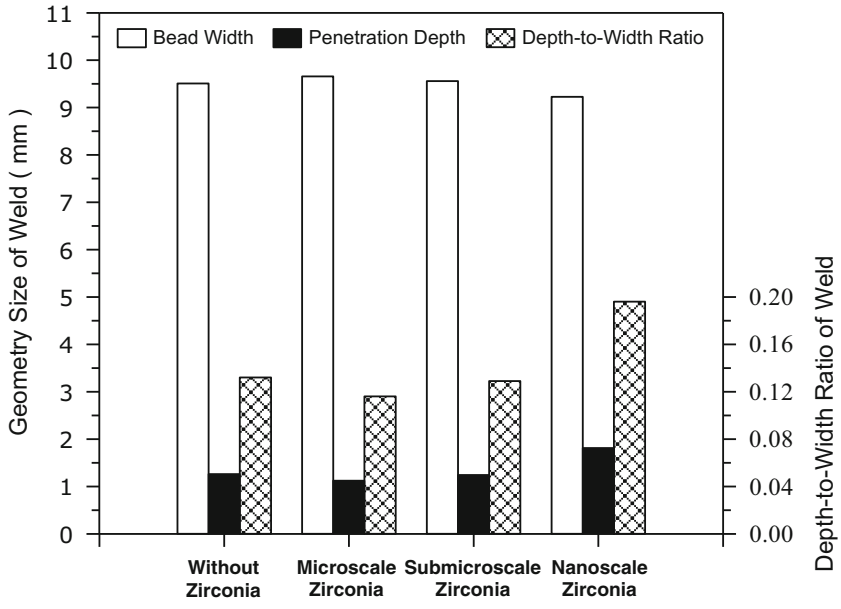

Fig. 4 Geometry size of TIG welds produced with and without ZrO_2 at a welding current of 200 A and a travel speed of 150 mm/min

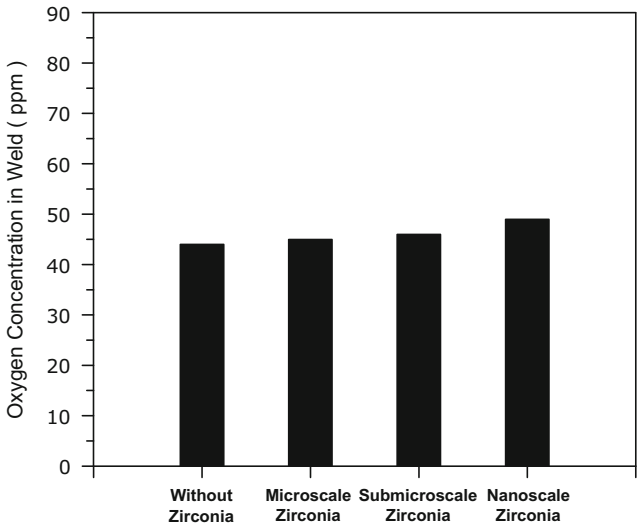

Fig. 5 Average oxygen concentration in AISI 316LN stainless steel TIG welds produced with and without ZrO_2 at a welding current of 200 A and a travel speed of 150 mm/min

In arc welding, the F_{em} is an important driving force for liquid metal flow in the welding pool. In TIG welding with a direct current electrode negative, the electric current in the specimen converges toward the tungsten electrode and, hence, near the center of the welding pool surface. This converging current field, together with the magnetic field it induces, causes downward and inward F_{em} in the welding pool. The liquid metal thus flows downward along the center of the welding pool and then upward along the boundary of the welding pool. As mentioned above, the use of microscale or submicroscale ZrO_2 flux formed ceramic slag, which indicates the screening action of electric current flowing through the welding pool surface. The ZrO_2 flux slag decreases the magnitude of the resultant F_{em} in the welding pool by reducing the density of electric current near the center of the welding pool surface, resulting in a shallow penetration depth.

Tseng and Lin [5] reported that the use of oxide with a less negative ΔG (such as SiO_2) and a small particle size can significantly increase the penetration depth compared with that achieved with the use of the same oxide with a large particle size. Tseng and Shiu [9] reported that the use of oxide with a more negative ΔG (such as Al_2O_3, MgO, or CaO) cannot increase the penetration depth of TIG weld. This study further showed that the use of oxide with a more negative ΔG (such as ZrO_2) and a small particle size cannot effectively increase the penetration depth and that the same oxide with a large particle size reduces the penetration depth. This trend is due to the thermodynamic stability of the oxide with more negative ΔG. It thus explains the radially outward direction of F_{tc} maintained in the welding pool. Moreover, the use of such oxide flux formed a heavy slag that floated on the welding pool surface, resulting in a weaker downward F_{em} in the welding pool.

3.3 Delta-ferrite content in TIG welds produced with different ZrO_2 particle sizes

Figure 6 shows the average δ-Fe content in AISI 316LN stainless steel TIG welds produced with and without ZrO_2 flux at a welding current of 200 A and a travel speed of 150 mm/min. The δ-Fe content is expressed in terms of ferrite number (FN). AISI 316LN stainless steel had an initial value of 0.1 FN. In the TIG weld produced without ZrO_2 flux, the average δ-Fe content in AISI 316LN stainless steel weld increased to 3.5 FN. This observation suggests that AISI 316LN stainless steel used in the present study solidifies as the primary δ-Fe phase and thus exhibits excellent weldability. The cooling rate substantially affected the δ-Fe content in austenitic stainless steel weld. When the cooling rate of austenitic stainless steel weld metal increased, transformation of the δ-Fe phase to the austenite (γ-Fe) phase had little time to occur, causing retention of more δ-Fe phase in the γ-Fe matrix after solidification. Compared with the TIG weld produced without ZrO_2 flux, TIG weld produced with microscale or submicroscale ZrO_2 flux retained less δ-Fe content. TIG welds produced with nanoscale ZrO_2 flux retained more δ-Fe. This study observed a slight increase in the δ-Fe content in TIG weld produced with nanoscale ZrO_2 flux as compared with that in TIG weld produced with microscale or submicroscale ZrO_2 flux. TIG welding with microscale or submicroscale ZrO_2 flux created a thermal barrier slag that floated on the welding pool surface, which trapped heat in the weld metal during solidification. The above results thus imply that the cooling rate of TIG weld produced with microscale or submicroscale ZrO_2 flux is lower than that of TIG weld produced without ZrO_2 flux. As a result, AISI 316LN stainless steel TIG weld produced with microscale or submicroscale

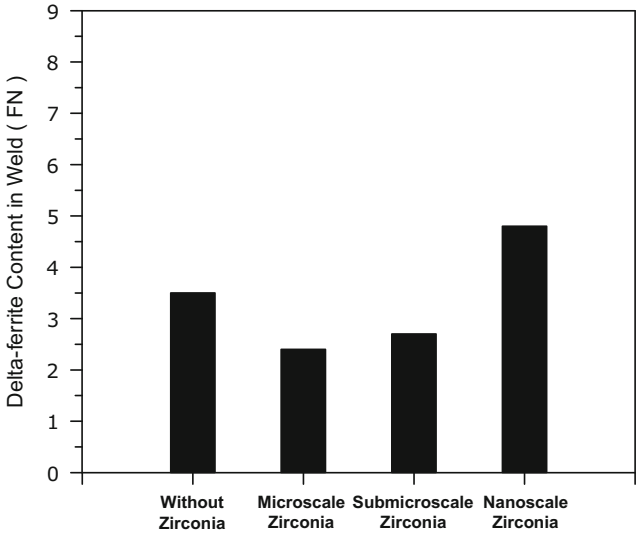

Fig. 6 Average delta-ferrite content in AISI 316LN stainless steel TIG welds produced with and without ZrO_2 at a welding current of 200 A and a travel speed of 150 mm/min

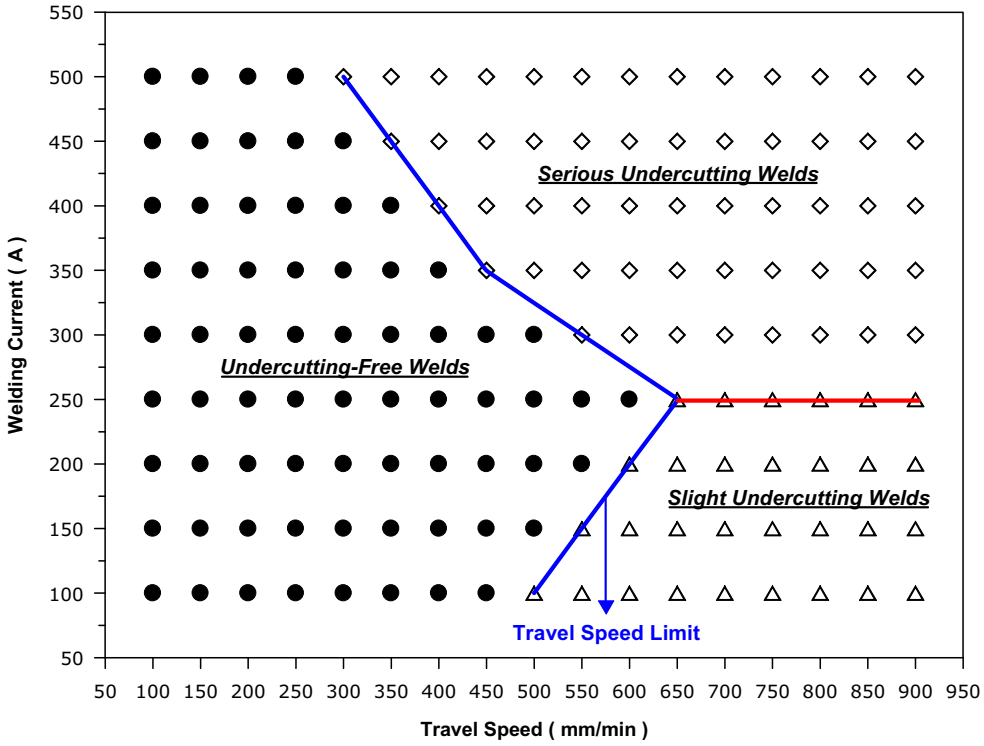

Fig. 7 Effect of travel speed limit on soundness of AISI 316LN stainless steel conventional TIG welds

ZrO_2 flux had δ-Fe content that is less than that of weld produced without ZrO_2 flux. In contrast to TIG welding with microscale or submicroscale ZrO_2 flux, TIG welding with nanoscale ZrO_2 flux produced a slag-free welded surface and thus a higher cooling rate, which resulted in greater δ-Fe content in AISI 316LN stainless steel TIG weld.

3.4 Potential advantages of ZrO_2-aided TIG welding

It is well known that travel speeds in fusion welding that exceed a certain limit result in an undercutting weld. That is, the maximum travel speed of fusion welding is restricted by the occurrence of undercutting defect. Figure 7 shows the effect of travel speed limit (TSL) on the soundness of AISI 316LN stainless steel conventional TIG welds. In this experiment, all bead-on-plate welds exhibited partial penetration. The weight per unit coated area of the microscale ZrO_2 flux was 3.23 mg/cm^2. The welding current (100–500 A range) and travel speed used (100–900 mm/min range) were increased in increments of 50 A and 50 mm/min, respectively. From this experiment, three ranges of current for conventional TIG welding could be identified: (i) at welding currents below 250 A, the TSL curve exhibited a positive slope, and undercutting welds formed at higher travel speeds; (ii) in the range of 250–350 A, the TSL curve exhibited a gradual negative slope. This current range represents a transition of weld geometry with respect to the effect of the arc pressure; (iii) at welding currents above 350 A, the TSL curve exhibited a steep negative slope, and undercutting welds formed at lower travel speeds. These results thus imply that undercutting defects were formed by high-speed, lower current fusion welding or by high-current, lower speed fusion welding.

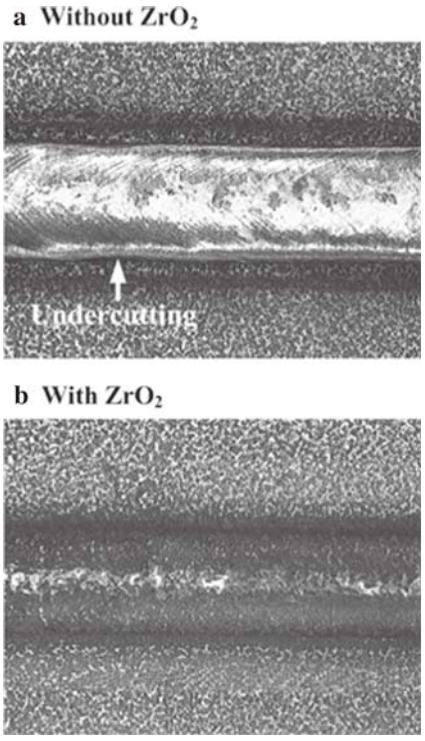

Fig. 8 Appearance of TIG welds produced with and without ZrO_2 at a welding current of 200 A and a travel speed of 600 mm/min

Figure 8 shows the appearance of TIG welds produced with and without ZrO_2 flux at a welding current of 200 A and a travel speed of 600 mm/min. The results show that a high-speed TIG weld produced without ZrO_2 flux at a welding current of 200 A results in a slight undercutting (Fig. 8a). The temperature difference across the welding pool surface was a key factor affecting undercutting formation [16]. When the travel speed of conventional TIG welding was too high, ripples at the surface of the solidified welds were very sharp (Fig. 9), resulting in a large difference in temperature between the center and edges of the welding pool surface. This result indicates that liquid metal near the center of the welding pool cannot promptly fill the welding pool edges before solidification. Thus, conventional TIG welding at a current below 250 A causes a large temperature difference across the free surface of the welding pool, resulting in a slight undercutting at the weld toe.

Development of high-speed welding process largely answers the need for increasing welding productivity without losing soundness of the welds. In this welding process, elimination of undercutting defect is a very important issue because it allows an increase in the maximum travel speed. Figure 8b shows the absence of undercutting when ZrO_2-aided high-speed TIG welding was done at a current of 200 A. As mentioned above, TIG welding with ZrO_2 flux created a ceramic slag that floated on the welding pool surface and trapped heat in the weld metal. As a result, the temperature difference between the center and edges of the welding pool surface decreased. This reduced the solidified rate of liquid metal at the welding pool edges and contributed to improvement of wetting of the liquid metal/solid metal interface, resulting in the elimination of undercutting defect.

The relationship between the welding current and TSL (Fig. 7) suggests that as the welding current exceeds 250 A, the slope of the TSL curve changes from positive to negative, resulting in a serious undercutting weld. This change indicates that travel speeds of high-current TIG welding beyond a certain limit lead to serious undercutting formation related to arc pressure. Notably, the arc pressure is the main function of the welding current and is independent of the travel speed.

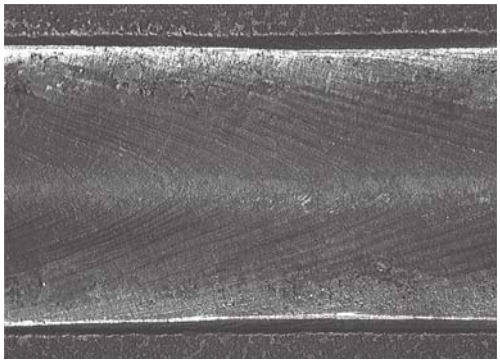

Fig. 9 Typical high-speed TIG welded surface with very sharp ripples

Figure 10 shows the appearance of TIG welds produced with and without ZrO_2 flux at a welding current of 350 A and a travel speed of 600 mm/min. The results show that a high-speed TIG weld produced without ZrO_2 flux at a welding current of 350 A results in a serious undercutting (Fig. 10a). When the welding current was below 250 A, the arc heat and liquid metal flow determined the weld geometry, with arc pressure apparently having little effect [11]. Upon increase of the welding current to above 250 A, the arc pressure increased gradually. The large arc pressure created a large gouged region at the front of the welding pool and forced the liquid metal to flow backward over the welding pool center. This increased the solidified rate of liquid metal at the rear of the welding pool, giving the backward-flowing liquid metal insufficient time to move back toward the welding pool edges. Thus, conventional TIG welding at a current above 250 A causes a large temperature difference across the welding pool surface and a large arc pressure at the front of the welding pool, resulting in a serious undercutting at the toe of the weld.

Figure 10b shows the absence of undercutting when ZrO_2-aided high-speed TIG welding was done at a current of 350 A. ZrO_2 flux was used to create a ceramic slag, which reduced the solidified rate of liquid metal at the rear of the welding pool and alleviated the arc pressure in front of the welding pool. This slag thus contributed to the liquid metal at the rear of the welding pool, which flowed into and filled the small gouged region because of the small arc pressure at the front of

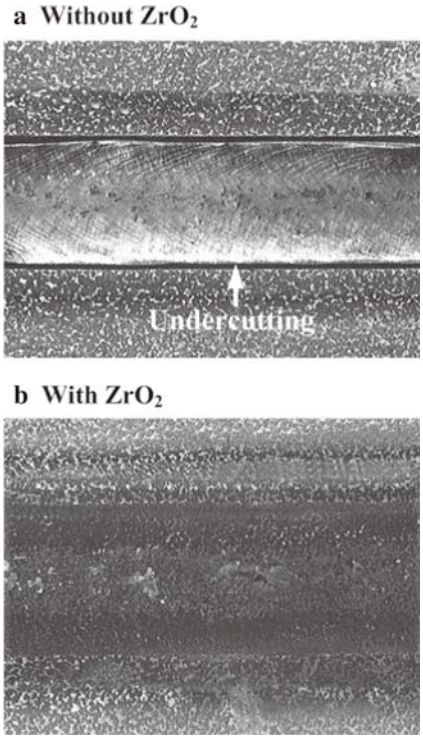

Fig. 10 Appearance of TIG welds produced with and without ZrO_2 at a welding current of 350 A and a travel speed of 600 mm/min

the welding pool. At the front of the welding pool, liquid metal flowing from the center to the edges had enough time to become smooth before solidification, thus eliminating the undercutting defect.

The results from this study show that ZrO_2 flux did not significantly contribute to an increase in the depth-to-width ratio of the weld, but it has low tendency to form undercutting and allows high-speed fusion welding. On the basis of the present results, high-speed TIG welding with a multicomponent ZrO_2-based flux (such as ZrO_2 + MoO_3 + Cr_2O_3 + SiO_2 + TiO_2) may be used to obtain a higher penetration depth of the weld with no undercutting. Although further investigation is necessary to understand the mechanism, the author hopes that the present study contributes to greater understanding of how ZrO_2 flux can be used to eliminate the undercutting defect of high-speed fusion weld.

4 Conclusions

TIG welding with different ZrO_2 particle sizes was performed to investigate the surface appearance, geometry size, and δ-Fe content of AISI 316LN stainless steel. The potential advantages of TIG welding with ZrO_2 flux were also demonstrated. The present work can contribute to better understanding of ZrO_2-aided high-speed TIG welding of stainless steel. The following conclusions based on our results have been reached:

1. Ceramic slag forms over the welded surface when using microscale or submicroscale ZrO_2 flux. Nanoscale ZrO_2 flux produces a slag-free surface of AISI 316LN stainless steel TIG weld.
2. Nanoscale ZrO_2 flux does not significantly contribute to an increase in the depth-to-width ratio of AISI 316LN stainless steel TIG weld.
3. Compared with the TIG weld produced without ZrO_2 flux, TIG weld produced with microscale or submicroscale ZrO_2 flux retains less δ-Fe content. This study observed a slight increase in the δ-Fe content in TIG weld produced with nanoscale ZrO_2 flux as compared with that in TIG weld produced with microscale or submicroscale ZrO_2 flux.
4. ZrO_2 flux may be used to create a ceramic slag that reduces the solidified rate of liquid metal and alleviates the arc pressure in the welding pool. This slag thus gives the liquid metal flowing in the center and edges of the welding pool enough time to become smooth before solidification, resulting in the elimination of undercutting defect.

Acknowledgments The author gratefully acknowledges the financial support provided to this study by the Ministry of Science and Technology, Taiwan under grant no. 104-2221-E-020-034.

References

1. Tseng KH, Chuang KJ (2012) Application of iron-based powders in tungsten inert gas welding for 17Cr-10Ni-2Mo alloys. Powder Technol 228:36–46
2. Tseng KH, Hsu CY (2011) Performance of activated TIG process in austenitic stainless steel welds. J Mater Process Technol 211:503–512
3. Tseng KH (2013) Development and application of oxide-based flux powder for tungsten inert gas welding of austenitic stainless steels. Powder Technol 233:72–79
4. Tseng KH, Chen KL (2012) Comparisons between TiO_2- and SiO_2-flux assisted TIG welding processes. J Nanosci Nanotechnol 12: 6359–6367
5. Tseng KH, Lin PY (2014) UNS S31603 stainless steel tungsten inert gas welds made with microparticle and nanoparticle oxides. Materials 7:4755–4772
6. Johnson MQ, Fountain CM (2003) Penetration flux. US 6664508B1
7. Muthukumaran V, Bhaduri AK, Raj B (2012) Penetration enhancing flux formulation for tungsten inert gas (TIG) welding of austenitic stainless steel and its application. US 8097826B2
8. Hu SS, Wang YH, Shen JQ, Chen CL (2013) Activating agent for argon tungsten-arc welding of ferritic stainless steel and application method thereof. CN 102554516B
9. Tseng KH, Shiu YJ (2015) Effect of thermal stability of powdered oxide on joint penetration and metallurgical feature of AISI 4130 steel TIG weldment. Powder Technol 286:31–38
10. Mendez PF, Eagar TW (2003) Penetration and defect formation in high-current arc welding. Weld J 82:269–306
11. Savage WF, Nippes EF, Agusa K (1979) Effect of arc force on defect formation in GTA welding. Weld J 58:212–224
12. Nguyen TC, Weckman DC, Johnson DA, Kerr HW (2006) High speed fusion weld bead defects. Sci Technol Weld Join 11:618–633
13. Pawlow P (1909) Über die Abhängigkeit des Schmelzpunktes von der Oberflächenenergie eines festen Körpers. Z Phys Chem 65:1–35
14. Tseng KH, Chen PY (2016) Effect of TiO_2 crystalline phase on performance of flux assisted GTA welds. Mater Manuf Process 31:359–365
15. Lu SP, Fujii H, Sugiyama H, Nogi K (2003) Mechanism and optimization of oxide fluxes for deep penetration in gas tungsten arc welding. Metall Mater Trans A 34:1901–1907
16. Tseng KH, Wang NS (2014) GTA welding assisted by mixed ionic compounds of stainless steel. Powder Technol 251:52–60